Fiber Tracking Method with Adaptive Selection of Peak Direction Based on CSD Model

Qian Zheng[1], Kefu Guo[2], Jiaofen Nan[3]*, Lujuan Deng[4], Junying Cheng[5]

College of Software Engineering, Zhengzhou University of Light Industry, Zhengzhou 450000, China[1, 2, 3, 4]
Department of Magnetic Resonance Imaging, the First Affiliated Hospital of Zhengzhou University, Zhengzhou 450000, China[5]

Abstract—As a multi-fiber tracking model, the constrained spherical deconvolution (CSD) model is widely used in the field of fiber reconstruction. The CSD model has shown good reconstruction capabilities for crossing fibers in low anisotropy regions, which can achieve more accurate results in terms of brain fiber reconstruction. However, the current fiber tracking algorithms based on the CSD model have a few drawbacks in the selection of tracking strategies, especially in the certain crossing regions, which may lead to isotropic diffusion signals, premature termination of fibers, high computational complexity, and low efficiency. In this study, we proposed the fiber tracking method with adaptive selection of peak direction based on CSD model, called FTASP_CSD, for fiber reconstruction. The method first filters the fiber orientation distribution (FOD) peak threshold and eliminates peak directions lower than the set threshold. Secondly, a priority strategy is used to implement direction selection, and the tracking direction is adaptively adjusted according to the overall shape and needs of the FOD. Through dynamic selection of the maximum peak direction, the second maximum peak direction and the nearest peak direction, the tracking direction that best matches the true fiber direction is found. This method not only ensures spatial consistency, but also avoids the influence of stray peaks in the FOD that may be introduced by imaging noise on the fiber tracking direction. Experimental results on simulation and in vivo data show that the fiber bundles tracked by the FTASP_CSD method have a much smoother in the overall visual effect than the state-of-the-art methods. The fiber bundles tracked in the region of crossing or bifurcating fibers are more complete. This improves the angular resolution of the recognition of fiber crossings and lays a foundation for further in-depth research on fiber tracking technology.

Keywords—Diffusion magnetic resonance imaging; constrained spherical deconvolution; fiber orientation distribution; fiber tractography

I. INTRODUCTION

White matter fibers are a critical component of the complex structure of the human brain, facilitating the exchange of information between different brain regions. The emergence of magnetic resonance diffusion tensor imaging technology has made it possible to study the morphology and distribution of white matter fiber bundles more effectively. Diffusion tensor imaging (DTI) [1] and white matter fiber tract tracking technology are commonly used in researching brain neurological diseases including, but not limited to apoplexy [2,3,4], schizophrenia [5,6], and multiple sclerosis [7,8]. By analyzing fiber bundles in different brain regions, researchers can reveal the mechanisms of neurological disease development

and pathological changes, providing more accurate information for the diagnosis and treatment of related diseases.

In recent years, the demand for increased accuracy in magnetic resonance imaging has grown due to rapid advancements in brain neuroscience. DTI is no longer sufficient for accurately reconstructing white matter nerve fibers as it can only represent fiber tracts with a single direction. To address this limitation, a series of high-angular resolution diffusion imaging (HARDI) methods have emerged to more accurately represent multiple fiber orientations within a single voxel. These methods can be broadly categorized as model-dependent or non-model-dependent. Model-dependent methods use complex models to describe multiple fiber orientation distributions. Examples of model-dependent methods include the multi-tensor model (MTM) [9,10,11], the ball and stick model [12], and constrained spherical deconvolution (CSD) [13,14,15] and others. Non-model-dependent methods, also known as q-space methods, are used to obtain the fiber orientation distribution function based on the Fourier transform relationship between the diffusion magnetic resonance signal and the diffusion tensor. These methods mainly include Q-ball imaging (QBI) [16,17], high-order tensor (HOT) model [18,19,20], and spherical harmonic (SH) function [21,22]. The CSD model is notable for its simple mathematical model and its ability to represent regions with multiple fiber orientations. It captures the primary fiber bundle structures identified by the DTI model, the CSD model and is also useful in delineating intricate fiber configurations, such as crossing and branching fibers. Therefore, the CSD model is a widely used method for solving complex fiber structures and has gained attention from researchers widespread. In 2004, Tournier et al. [14] initially introduced a deconvolution algorithm that uses spherical harmonics to improve the accuracy of fiber direction information. This method aims to improve the accuracy of fiber direction information by leveraging the linear transformation relationship between the HARDI acquisition signal and the fiber direction di distribution function. However, the algorithm faces some challenges. Firstly, the high-frequency noise introduced by the signal acquisition process results in unnecessary negative values in the solution of the spherical inverse convolution model. In addition, the acquired signals limit the improvement of the spherical harmonic order, making it difficult to identify fiber crossing problems at small angles. To address these issues, in 2007, Tournier et al. [13] attempted to filter the high-frequency components of the spherical harmonics to improve noise immunity. However, this approach also results in a decrease in the angular resolution of the model. Subsequently, Patel et al. [23] proposed an iterative negative value adjustment method. This method makes the direction

---

distribution function approach the non-negative domain through multiple iterations. However, due to the non-negativity of the solution space, it cannot be guaranteed that the noise will not increase as the angular resolution increases. In 2010, Calamante et al. [24] further proposed a super-resolution spherical deconvolution method to improve angular resolution and suppress noise to a certain extent. However, this method requires signals to be acquired in multiple gradient directions, involves a large number of calculations, and has a high order, making it unsuitable for clinically complex fiber structure reconstruction. Although the above model provides estimates of fiber orientation in white matter regions, it may produce inaccurate orientation estimates in voxels containing other tissue types (Gray matter, Cerebrospinal fluid). In 2014, Jeurissen et al. [25] proposed a multi-shell multi-tissue constrained spherical deconvolution model to solve this problem. The model simulates the main tissue types present in the brain, namely white matter, gray matter, and cerebrospinal fluid. It improves the difficulty in distinguishing multiple tissue types when using single-shell data in the past. By using multi-b-value data, exploiting the dependence of different tissue types on different b-values provides the CSD model with the opportunity to distinguish the contribution of each tissue type.

There are many tracking algorithms based on the CSD model in the field of fiber tracking due to the superiority of the CSD model [26, 27, 28]. However, most of these algorithms adopt a probabilistic tracking strategy [27, 28], which can cause premature termination of fiber tracking at the white matter boundary. Moreover, the algorithm also requires a large number of random samples, resulting in low efficiency due to the high computational demand. Therefore, this paper proposed a new deterministic fiber tracking strategy based on the CSD model. This method uses multi-b value data to solve the CSD model based on estimating the tissue response function to obtain the fiber orientation distribution (FOD). Calculate the maximum and second maximum peak directions of FOD, and give priority to the maximum and second maximum peak directions as the tracking direction of the current voxel. This is because the peak direction in FOD represents the degree of contribution of fiber bundles, and the larger the peak direction, the more likely there are fiber bundles. If the angle between the largest and second largest peak directions and the previous step tracking direction is too large or the direction is opposite, then the peak direction with the greatest cosine similarity between the FOD peak direction and the previous step tracking direction, that is, the nearest peak direction, is selected as the fiber tracking direction. If neither is satisfied, the tracking will be terminated. The algorithm in this paper adaptively selects the tracking direction based on the overall shape of the FOD and historical tracking direction information to improve tracking accuracy and efficiency and better reveal the fiber structure in diffusion MRI data.

II. METHODS

The FTASP_CSD method involves several steps, including data preprocessing, extract gray and white matter boundaries, estimate response function, solving the CSD model to obtain the fiber orientation distribution, and performing the fiber tracking. The technical roadmap of the FTASP_CSD method is given in Fig. 1.
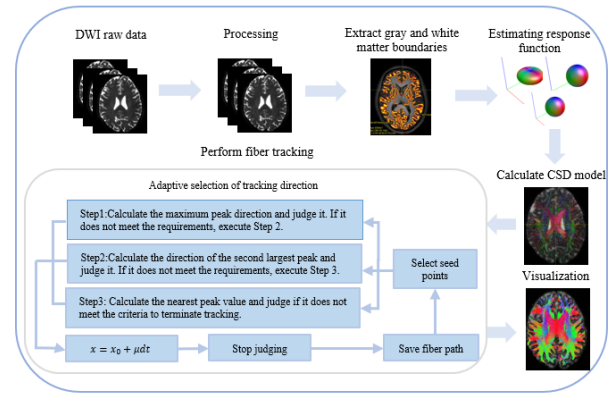

Fig. 1. Fiber tracking technology roadmap.

A. Solve the CSD Model

The CSD model typically considers the overall diffusion signal as the convolution of the response function of a single fiber signal and the probability density function of the fiber direction on the sphere, as described in references [29, 30]. In the case where only one continuous fiber exists, the measured DW-MRI signal is called the signal response function, represented by R, which is an axially symmetric matrix. When multiple fibers are present in a single voxel, the measured DW-MRI signal can be expressed as the convolution of the FOD and the signal response function on a sphere, as shown in Eq. (1).

$$S = \frac{S(g)}{S_0} = \int_{S^2} R(g,r) \cdot F(r) dr = R(g,r) \otimes F(r)$$

(1)

where, $F(r)$ is the directional probability density function on the unit sphere, representing the size of the fiber distribution in each direction. g is the direction of the unit diffusion impulse gradient $S(g)$ is the measured signal at the direction of the impulse gradient, S_0 is the measured signal when there is no impulse gradient, S^2 is the domain of the integrating sphere, and r is the unit direction vector.

The weight coefficient of the fiber direction can be determined using Eq. (2) and Eq. (3).

$$A_{ij} = \int R_i(g,r) F_j(r) dr \qquad (2)$$

$$f = \arg\min\left\{\|Af - y\|^2\right\} \qquad (3)$$

When collecting data using diffusion magnetic resonance imaging equipment, the number of collected gradient directions is limited. This limitation may result in significant deviations in the results when using the optimal solution described in Eq. (3). To address this issue, Tournier et al. proposed the CSD method, which introduces a penalty parameter λ and a constraint matrix T of the smooth solution set to redefine the coefficient solution process, as shown in Eq. (4).

$$f = \arg\min\left\{\|Af - y\|^2 + \lambda^2 \|T f\|^2\right\} \qquad (4)$$

B. The Proposed FTASP_CSD Method

Fiber tracking technology is a non-invasive method used to reconstruct the neural fiber bundles in the brain's white matter. The FOD is leveraged to estimate the properties of white matter tissue and extract its structural orientations. This directional information is then used by fiber tracking algorithms to obtain microstructural details of white matter tissue, enabling the three-dimensional reconstruction of neural fiber bundles. The FTASP_CSD method adopts a streamline iterative approach, adapting the tracking direction based on the overall shape and requirements of the FOD. Before selecting the tracking direction, the experiment first evaluates the FOD peak. If the amplitude is less than the specified threshold, tracking is terminated. The selection of this threshold should avoid stray peaks introduced by imaging noise in the FOD while ensuring adherence to the true direction of fiber extension. In this study, the threshold was set to 0.1, which is an empirical value that generally yields satisfactory results in most cases [31,32]. This determination is based on visual inspection of white matter fiber tracking results and comparison with known anatomical structures.

In mathematical terms, the deterministic tracking algorithm can be viewed as a form of initial value problem in ordinary differential equations. The trajectory of the fiber bundle in three-dimensional space is defined as $x(p)$, expressed as $p \rightarrow x(p)$ in Eq. (5).

$$\begin{cases} \dfrac{dx(p)}{dp} = e\left[x(p)\right] \\ x(0) = x_0 \end{cases} \qquad (5)$$

where, e is the fiber pathway direction at point p, and x_0 is the seed point of the fiber tracking.

The fiber path can be iteratively tracked by using the Euler method to solve the formula mentioned above, as described in Eq. (6).

$$x_{p+1} = x_p + t d_p \qquad (6)$$

where, t is the step size, usually a constant with $t > 0$, and d_p represents the current voxel's fiber tracking direction. The cosine similarity θ between the current voxel and the previous voxel's progression direction is calculated using the dot product and vector lengths, the change in d_p can be determined based on the value of θ, as shown in Eq. (7).

$$\cos(\theta) = \frac{\varepsilon_p \cdot d_{p-1}}{\|\varepsilon_p\|\|d_{p-1}\|} \qquad (7)$$

Let $\varepsilon_p = [\varepsilon_1, \varepsilon_2, \ldots]$ is peak directions of the voxel at position x_p. Let v_1 be the maximum peak direction and v_2 be the second maximum peak direction at the current voxel, as shown in Eq. (8).

$$v_1 = Max\{\varepsilon_p = [\varepsilon_1, \varepsilon_2, \ldots]\}$$

$$v_2 = Second\{\varepsilon_p = [\varepsilon_1, \varepsilon_2, \ldots]\} \qquad (8)$$

For the selection criteria of peak directions, a judging parameter is defined, as shown in Eq. (9).

$$C = |v_t \cdot v_{t-1}| \qquad (9)$$

where, v_t is the unit vector of the currently selected peak direction at the voxel, and v_{t-1} is the direction of the previous fiber tracking step. C represents the magnitude of the angle between the peak direction and the previous fiber tracking direction. The threshold for C is set to 0.7 (approximately 45°). If C is less than 0.7, it is considered that the selected peak direction has a too large deviation angle.

The direction selection in fiber tracking employs a priority strategy. If the maximum peak direction aligns with the previous tracking direction, the maximum peak direction v_1 is prioritized as the fiber tracking direction. This is because the FOD describes the distribution of possible fiber bundle directions at the voxel, and the value of each direction component represents the strength of the corresponding fiber bundle contribution. A larger magnitude typically corresponds to a higher weight, with the maximum peak direction representing the primary fiber bundle direction. If the angle between the maximum peak direction and the previous tracking direction is excessively large or opposite to the previous tracking direction, the secondary peak direction v_2 is considered. Similarly, judgment is made for the secondary peak direction, and if it does not meet the criteria, other lower-amplitude peak directions are not considered further. This is because other peak directions generally have lower weights and may introduce numerous false streamlines affected by noise. If neither the maximum nor the secondary peak directions are satisfied, according to anatomical research and clinical observation, white matter fiber continuity and angle bending have certain conventions. The pathway of white matter fibers typically undergoes appropriate angles of bending along its course. Therefore, the peak direction d_p closest to the previous tracking direction is chosen as the next tracking direction. If it still does not meet the tracking requirements, tracking is terminated. This approach ensures the continuity of tracking paths and prevents excessive jumps or discontinuities. This strategy fully utilizes the information from the FOD, enabling the fiber tracking algorithm to accurately and reliably reconstruct the trajectory of white matter fiber bundles in three-dimensional space. This approach ensures the continuity of tracking paths, preventing excessive jumps or discontinuities.

This strategy fully leverages the information from the FOD, enabling the fiber tracking algorithm to reconstruct the trajectory of white matter fiber bundles accurately and reliably in three-dimensional space.

The fiber tracking path of the nearest peak direction can be depicted by Fig. 2. x_0 represents a randomly selected seed point within the FA threshold, and d_p represents the fiber tracking direction. At the point x_2, θ represents the cosine similarity, and d_p is the tracking direction of the current point.
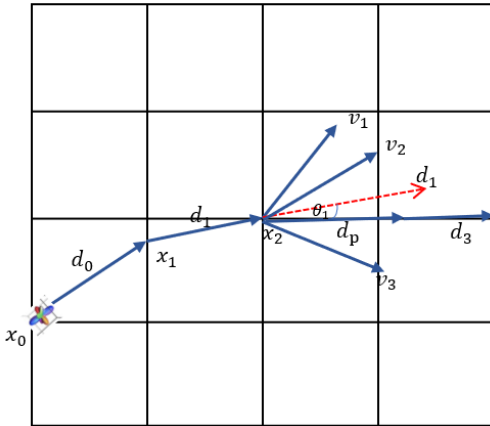

Fig. 2.   The process of tracking the nearest peak direction.

To prevent tracking overfitting, it is necessary to set termination criteria for fiber tracking. Typically, the tracking process is terminated when the local FA or the curvature of the tracking direction falls below a predefined threshold. The process of the fiber tracking method is illustrated below.

Algorithm: The specific process of the FTASP_CSD

Step 1: Select the seed point x_0, traverse the FOD at x_0 and find the peak direction.

Step 2: Let $x_p = x_0$, $d_p = d_0$, execute $x_1 = x_0 + \mu d_0$.

Step 3: Determine whether the voxel FOD peak threshold is greater than the set minimum threshold 0.1. If it is less than the set minimum threshold, the tracking will be terminated.

Step 4: If satisfied, calculate the cosine similarity between $\varepsilon_p = [\varepsilon_1, \varepsilon_2, ...]$, select the maximum peak direction and the second maximum peak direction.

Step 5: Determine the angle between the unit vector of the maximum peak direction and the previous tracking direction. If it meets the requirements, extend along the maximum peak direction as the tracking direction; otherwise, consider the second maximum peak direction.

Step 6: If the second maximum peak direction of the FOD meets the requirements, extend along the second maximum peak direction as the tracking direction. Otherwise, calculate the cosine similarity between $\varepsilon_p = [\varepsilon_1, \varepsilon_2, ...]$ and d_{p-1}.

Step 7: Select the peak direction v_1 with the maximum cosine

---

similarity to the previous tracking direction d_{p-1}.

Step 8: Check if v_1 exceeds the set threshold value. If it is smaller than the threshold, continue tracking; otherwise, terminate the process.

Step 9: Advance one t in turn to the next voxel.

Step 10: $p = p + 1$, repeat steps 3 to 9 until the stopping criteria are met to obtain a continuous fiber path.

III. RESULTS

To evaluate the good performance of the FTASP_CSD, this paper uses Matlab as the platform. The proposed method is benchmarked against several state-of-the-art techniques, including the fiber assignment by continuous tracking (FACT) [33], the tensor deflection algorithm (TEND) [34], the streamlines tractography based on spherical deconvolution (SD_Stream) [26], the second-order integration over fiber orientation distributions (iFOD2) [27] and anatomically-constrained tractography second-order integration over fiber orientation distributions (ACT_iFOD2) [28]. FACT and TEND adopt the DTI model, while the SD_Stream, iFOD2, ACT_iFOD2, and the proposed FTASP_CSD algorithms all adopt the CSD model. The Fibercup simulation data and in vivo human brain data are used to verify the performance of the proposed FTASP_CSD method. The presence of significant random noise, artifacts, and geometric distortion caused by magnetic susceptibility in diffusion-weighted imaging (DWI) images can impact the accuracy of fiber tracking and result in interruptions to the process. To improve the accuracy of DWI data before fiber tracking, a series of preprocessing steps must be performed. This includes obtaining a more accurate binary mask image, which will improve tracking accuracy and result in a more continuous fiber bundle path. The experiment utilized the same preprocessing steps for both the simulated and in vivo datasets, and the preprocessing was implemented on the MRtrix platform (https://www.mrtrix.org/). The pre-processing steps for DWI images are as follows.

Step 1: Denoising DWI. The original DWI data contains noise and distortion, which can be reduced by using the denoise command. This command estimates the MRI noise level and applies denoising based on random matrix theory.

Step 2: Removal of Gibbs artifact. This artifact, also known as truncation artifact, is related to spatial resolution. It is well known that an image consists of small pixels and contains an infinite number of spatial frequencies, but the system only collects image signals at a limited number of frequencies leading to Gibbs artifacts, which can be removed from DWI images using local sub-voxel displacement methods.

Step 3: Correction DWI distortion using dwifslpreproc. This corrects the geometric distortion caused by the magnetic susceptibility present in the diffusion image, as well as any distortion caused by eddy currents and the subject's main body motion, and this step depends on the FSL command.

Step 4: Correction of b_1 field inhomogeneity for a DWI volume series. This step aims to improve brain mask estimation. However, if there are no strong bias fields present in the data,

running this script may worsen brain mask estimation and result in an inferior outcome.

A. Simulation Study

The Fibercup simulation data used in this paper was provided in a challenge sponsored by the medical image computing assisted intervention society (MICCAI) in 2009. The small data volume of this Fibercup data from https://tractometer.org facilitates rapid acquisition of fiber information and the calculation of quantitative metrics. The data contains 64 diffusion gradient orientations, the brain slices are $3mm \times 3mm \times 3mm$ in size, with a voxel volume of $64 \times 64 \times 3$. The Fibercup data contains five different fiber types, mimicking the many complex structures of real fiber bundles in the brain (crossings, sectors, bifurcations, etc.), as shown in Fig. 3. The blue background is the mask of the Fibercup data.
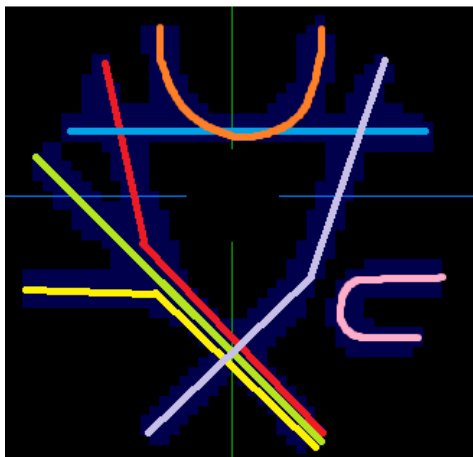

Fig. 3. The model diagram of fiber crossing and branching regions.
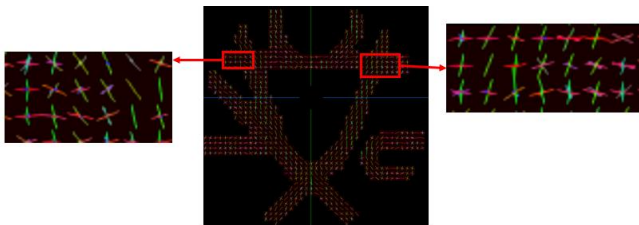

Fig. 4. The reconstruction results of the FOD.

We reconstructed the FOD of the simulated data described above using the CSD model. The peak values of FOD at each voxel represent the fiber orientations. The FTASP_CSD method utilizes these peak values to reconstruct the white matter neural fibers in the brain. To provide a clearer description of the fiber orientations, we visualized the peak values of voxels based on FOD, and the reconstruction results are shown in Fig. 4. From an overall visual perspective, the CSD model accurately reconstructs the diffusion model of crossing structure voxels. Additionally, for voxels containing three or more crossing fibers, the model also effectively reconstructs multiple peaks.
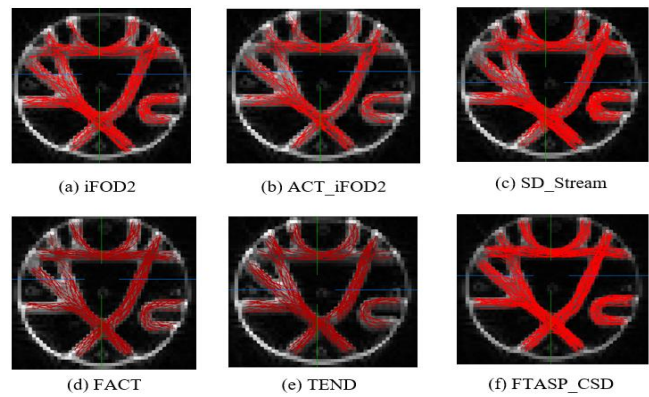

Fig. 5. Comparison of tracking effects with various tracking methods on the simulated dataset.

Fiber tracking experiments were conducted on the masked region using Fibercup data based on the FOD. The experimental results are shown in Fig. 5. It shows that the FACT and TEND algorithms based on the DTI model produce relatively coarse tracking results. In regions of crossings and bifurcations, partial fiber bundle losses occur, resulting in low fiber coverage. These limitations in tracking crossing fiber bundles are inherent to the DTI model. However, the DTI-based algorithms perform well in tracking the main pathways of fiber bundles. In contrast, algorithms that rely on the CSD model, such as SD_Stream, iFOD2, and FTASP_CSD, provide greater coverage of fiber bundles compared to other algorithms. The illustration shows that the SD_Stream algorithm is capable of tracking most fiber bundles, but has limitations in tracking U-shaped fiber bundles compared to the FTASP_CSD method. Both the iFOD2 and ACT_iFOD2 algorithms produce a relatively lower count of complete fiber bundles due to the probabilistic nature of fiber tracking. The ACT_iFOD2 algorithm tracks significantly fewer fiber bundles than the iFOD2 algorithm. This is attributed to the addition of anatomical constraint steps to the iFOD2 algorithm, a method designed to filter out erroneous fibers but simultaneously lead to the removal of valid fibers. The FTASP_CSD method yields fiber direction that is relatively consistent with the white matter structure distribution of the diffusion image associated with high coverage and high smoothness. Tracking does not exhibit premature termination or exceeding the boundary.

After obtaining the distribution of the fiber bundle, use Tractometer [35] to calculate quantitative indicators for the results of different tracking algorithms. The Tractometer is an independent evaluation tool of the ISMRM2015 Challenge, which was used to evaluate and compare the performance of fiber tracking methods quantitatively. Tractometer provides quantitative measures such as invalid bundles (IB), invalid connections (IC), no connections (NC), valid connections (VC), and average bundle coverage (ABC), among others. These quantitative results are displayed in Fig. 6.
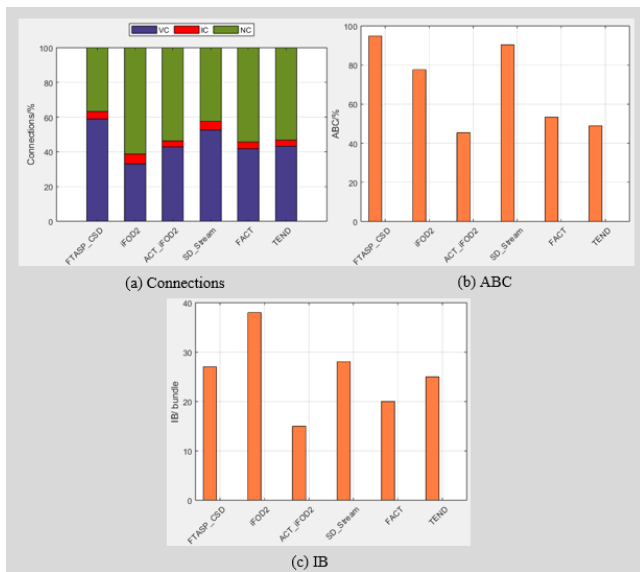
Fig. 6. Comparison of quantitative results with different tracking methods on simulation data.

Fig. 6 demonstrate that the method proposed in this study outperforms other tracking algorithms based on the CSD model in terms of higher accuracy. Compared to algorithms based on the DTI model, the proposed method also shows superior performance in certain metrics. Among the algorithms based on the CSD model, the FTASP_CSD method tracks the fewest invalid fiber bundles, demonstrating superiority over other algorithms, except for the ACT_iFOD2 algorithm. In contrast, the iFOD2 algorithm performs the least favorably in terms of the quantity of invalid fiber bundles. Compared to CSD model algorithms, the DTI model-based FACT and TEND algorithms exhibit a lower number of invalid fiber bundles. Regarding the fiber connection ratio, the FTASP_CSD achieves the highest VC and the lowest NC among the six algorithms. On the contrary, the iFOD2 algorithm performs the least favorably in terms of the NC. Compared to CSD-based algorithms, DTI-based algorithms exhibit a higher NC, with the FACT and TEND algorithms having very similar IC. In terms of fiber coverage, it has been found that fiber tracking algorithms based on the CSD model outperform those based on the DTI model. The FTASP_CSD achieves the highest fiber coverage among CSD model algorithms, reaching almost 95%. In contrast, the ACT_iFOD2 algorithm has the lowest fiber coverage, at just under 46%. A comprehensive analysis indicates that the FTASP_CSD method is superior to the other five algorithms in terms of fiber reconstruction. This advantage is especially noticeable in aspects such as the number of IB, VC, and ABC, which provide a more accurate and comprehensive solution for fiber tracking algorithms based on the CSD model.

B. Clinical Study

The clinical dataset used in this study was obtained from the Medical Image Analysis and Statistical Interpretation (MASI) laboratory [36]. 50 MRI cases were used to compare the proposed method in this paper with five other algorithms. Each subject underwent scans with identical parameters. The brain slices of the data were $2.14mm \times 2.14mm \times 2.2mm$, with a total brain size of $112 \times 112 \times 54$. The dataset comprised 96 DWI images with applied directional gradient pulses and 16 DWI images without applied directional gradient pulses. The b-values included $b = 1000s/mm^2$ and $b = 2000s/mm^2$. To validate the effectiveness of the algorithm, we selected both the entire brain region and the corpus callosum (CC) region as regions of interest for tracking. Fiber tracking was performed using the FTASP_CSD method and five other commonly used tracking algorithms. The tracking results were then evaluated, and statistical analyses were conducted on the outcomes.

Whole-brain fiber tracking uses brain white matter as the area of interest. The seed point is located in the mask area of the brain white matter. The seed point area of the whole brain is shown in Fig. 7.

Fig. 7. Seed point region of the whole brain.

The whole brain fiber tract represents the direction of nerve fibers in the entire brain, one example was selected to visualize the fibers in the entire brain. The fiber tract tracking of the whole brain is shown in Fig. 8. For better visualization of the overall fiber tracking results, they were overlaid onto diffusion-weighted imaging data for presentation. From Fig. 8, it can be observed that several algorithms effectively tracked the symmetric structures of the whole brain, reconstructing the overall trajectory of brain fibers. However, in terms of fiber distribution, the CSD model tracking algorithm exhibited an advantage, providing more comprehensive information for fiber reconstruction. It can be seen from the figure that the FTASP_CSD method, iFOD2 algorithm, and SD_Stream algorithm cover a wider range of white matter areas in diffusion images than other algorithms, especially the FTASP_CSD method with the highest coverage. Although the ACT_iFOD2 algorithm is also implemented based on the CSD model, in the algorithm ACT uses the gray-white matter junction as the starting point or cutoff point for fiber tracking, so the results will be eliminated, and some erroneous fibers may be eliminated, and some effective fibers may be eliminated. However, the FACT algorithm and TEND algorithm based on the DTI model have some fiber loss in the edge area of the diffusion image, especially at both ends of the diffusion image. This is related to the limitations of the DTI model itself. In terms of smoothness and continuity, the FTASP_CSD method adds consideration to the historical tracking direction, considers the selection of the peak direction in multiple directions, and filters the peak threshold. This promotes fiber tracking smoothness and avoids premature fiber termination to a certain extent. Therefore, the FTASP_CSD method also performs optimally in terms of fiber smoothness and continuity.
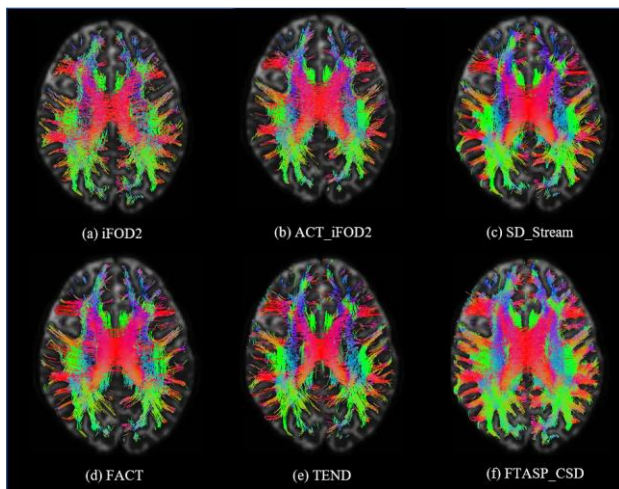
Fig. 8. Comparison of whole-brain fiber tracking results of various tracking methods.

TABLE I. STATISTICAL COMPARISON OF THE WHOLE BRAIN TRACKING FIBER RESULTS WITH THE SIX METHODS ($\bar{x} \pm S$)

Method	FB_num	FL_max	FL_min	FL_mean	Time
FACT	22700±2132	226.59±16.61	20±3.11	50.79±10.63	61±3.6
TEND	15564±943	259.39±8.95	20.99±4.81	55.75±12.6	64±4.1
SD_Stream	29697±2854	200.39±6.44	20.18±5.25	38.37±3.18	126±6.4
iFOD2	31104±1119	189.21±5.19	20.22±5.60	38.59±4.27	129±4.7
ACT_iFOD2	24753±1536	198.65±9.72	24.25±9.25	40.45±8.07	159±6.9
FTASP_CSD	38132±2861	216.80±11.75	22.54±5.42	48.44±10.8	176±9.0

Note: FB_num is the number of fibers, FL_max is the longest fiber length, FL_min is the shortest fiber length, and FL_mean is the average fiber length.

Since there is no Ground Truth in clinical data, the Tractometer quantitative index calculation is no longer performed on the clinical data results. Only the statistical parameters of the whole-brain tracking results of 50 subjects are displayed in the form of mean ± standard deviation, as shown in Table I. The results indicate significant differences between the tracking algorithm based on the DTI model and the tracking algorithm based on the CSD model. The DTI model-based algorithm shows that the FACT and TEND algorithms track fewer fibers, but the average and the longest fiber lengths are longer compared to the algorithm of the CSD model and the time consumed is short. From the perspective of the CSD model-based algorithms, the tracking algorithms based on the CSD model track the number of fiber strips more comprehensively due to the characteristics of the CSD model, which can obtain a more comprehensive fiber distribution. Specifically, the average number of fibers tracked by the iFOD2 algorithm is about 6351 less than that of the ACT_iFOD2 algorithm. This is because the ACT_iFOD2 algorithm adds an ACT step and removes erroneous fibers from the iFOD2 tracking results. The FTASP_CSD method tracks the largest number of fiber bundles,

and its average length has reached the level of the DTI model. In terms of time consumption, it is also the shortest among several CSD model-based algorithms, second only to the FACT and TEND algorithms. Its duration is within the acceptable range for clinical application. Therefore, it can be concluded that the FTASP_CSD achieves both the running time of the tracking method based on the DTI model and the number of fibers tracked based on the CSD model, perfectly integrating the advantages of the both.

Due to the large number of nerve fiber bundles in the whole brain, the differences between the algorithms are not obvious enough. Therefore, in order to more accurately observe and analyze the reconstruction results of nerve fiber bundles, the corpus callosum area was selected as the area of interest to conduct fiber tracking experiments. The red area is the seed point area of CC, as shown in Fig. 9.
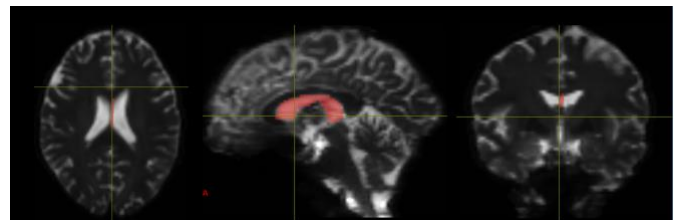

Fig. 9. The seed-point region of the corpus callosum.

The tracking results of different tracking algorithms in the corpus callosum area are shown in Fig. 10. As can be seen from Fig. 10, the tracking algorithm based on the DTI model can well track the main fiber bundles of the corpus callosum, but the tracking effect has limitations in the fiber cross-bifurcation area, such as not tracking the fibers on both sides of the corpus callosum. Comparing the six algorithms, the iFOD2 algorithm obtained the largest number of fibers, but the corresponding number of erroneous fibers was also the largest and most scattered. The ACT_iFOD2 algorithm added an anatomical constraint step based on the iFOD2 algorithm and eliminated some erroneous fibers, resulting in a significant reduction in fibers, which also reversely confirms that most of the wrong fibers exist in iFOD2. However, the algorithm still has some incorrect fibers at the end, such as the extra blue fiber bundle at the end, which does not exist in anatomy. The SD_Stream algorithm can track the general direction of the fiber tracts and reconstruct most of the fiber tracts in the corpus callosum, without erroneous blue fiber tracts appearing at the ends. However, some fiber bundles are missing on the left side of the corpus callosum, and the tracking is incomplete. The FACT algorithm tracks the smallest number of fibers, but the main direction of the fibers is very clear. The TEND method performs well in terms of smoothness, but both the TEND algorithm and the FACT algorithm have obvious blue error fibers at the ends. The FTASP_CSD method can track the fiber tracts in the corpus callosum area very well, especially the red fiber tracts connecting the left and right brain areas. It is more complete than other algorithms and does not have obvious erroneous fibers. The main direction of the fiber is more obvious, and the smoothness is also better.
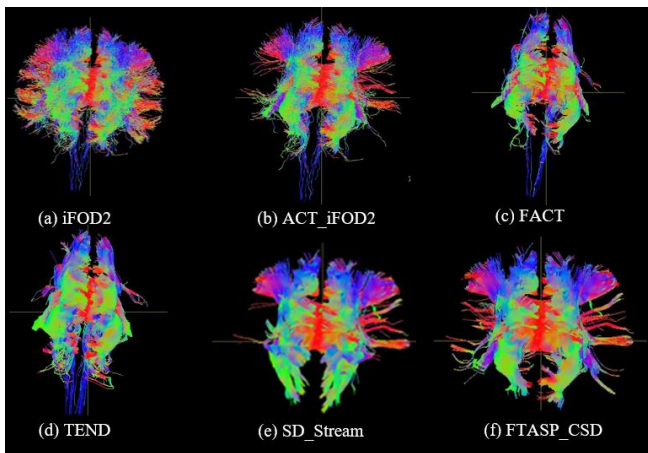
Fig. 10. Comparison of tracking effects in the corpus callosum region with various tracking methods on clinical data.

IV. DISCUSSION

In this work, we primarily conducted experiments on simulation dataset and vivo dataset, which demonstrated the feasibility of the FTASP_CSD method. Specifically, this method achieved superior performance in both datasets. From visual inspection, FTASP_CSD performs better than other algorithms in fiber crossing and branching regions, and can achieve more reliable fiber reconstruction results. From the statistical results, the FTASP_CSD method achieves the highest VC and the lowest NC among the six algorithms. Moreover, the results show that the tracking time of the algorithm in this article is shorter than the other three algorithms based on the CSD model in the article, reaching the level of the DTI-based algorithm.

The fiber tracking algorithm, which is based on the DTI model, has a single model and can only achieve better tracking results in areas with relatively high anisotropy. In complex fiber regions, the distribution of fibers in all directions may cause the FA of a voxel to be very small or even isotropic, which may be mistaken for the absence of fiber tracts in that voxel. Therefore, both the FACT algorithm and the TEND algorithm on Fibercup simulated data demonstrate more accurate tracking in a single direction, while tracking fewer fibers in complex fiber regions. However, some crossing and branching fiber bundles may not be tracked. On the real human brain dataset, it is evident that there is a loss of fibers on both sides in the tracking region, with only the major fiber bundles being reconstructed. The CSD model serves as a multi-fiber tracking model, and that can depict directional information in complex regions. Therefore, despite being a deterministic fiber tracking algorithm, the SD_Stream algorithm can achieve favorable tracking results in regions with complex fiber distributions. The SD_Stream algorithm and TEND algorithm share a common fiber curve iteration approach, both iterating the tracking direction as the tangent direction of the fiber curve. In contrast, FACT directly employs the tracking direction as a straight segment of the fiber curve within the voxel, resulting in poor smoothness in the tracking results. The iFOD2 algorithm selects the tracking direction of fibers through orientation distribution function sampling. In this mode, different fiber directions are potentially selected, resulting in a more comprehensive tracking of fibers. However, it generates a

substantial number of spurious fibers. This characteristic leads to the highest IB for fibers and relatively highest ABC as shown in Fig. 6. The ACT algorithm filters the tracking results of fibers directly, using anatomical constraints to eliminate erroneous fiber bundles. This is evident in both simulated and real datasets, where the ACT_iFOD2 algorithm tracks fewer fiber bundles compared to iFOD2. Simulation study on the Fibercup dataset shows that ACT eliminates a considerable number of fiber bundles, including some reasonable ones, resulting in the lowest ABC. Additionally, this dataset produces outcomes that are consistent with real human brain data. The FTASP_CSD method is based on the CSD model and adopts a tracking strategy that adaptively selects the peak direction. Therefore, it has achieved excellent results in the fiber intersection and bifurcation areas of Fibercup data and real human brain data. For instance, in the Fibercup dataset, it is noticeable that the tracked fiber quantity remains relatively high in areas of fiber crossing and branching, with the ABC having the highest quantity compared to other CSD models. In the vivo study, it is evident that the FTASP_CSD method effectively tracks the crossing fiber bundles on both sides of the corpus callosum region. The tracking direction strategy of this method not only considers the main fiber bundle distribution direction, but also considers the influence of the previous step tracking direction on the current voxel peak direction. Moreover, the peak threshold is limited to reduce the impact of spurious peaks caused by noise on the tracking results. By adaptively selecting the peak as the tracking direction, the maximum probability fiber direction distribution tracking is changed, and the generation of erroneous fibers is reduced on the basis of increasing the number of fiber bundles. Therefore, this method has the smallest IB value compared to the iFOD2 and SD_Stream algorithms. In addition, because the influence of the historical tracking direction on the voxel direction is considered, the continuity and smoothness of fiber bundles tracked by the FTASP_CSD method are also better than those of iFOD2, ACT_iFOD2, and SD_Stream algorithms.

As demonstrated in the experiments, the FTASP_CSD method produces favorable results on both simulated and real human brain datasets. However, two limitations need to be noted regarding the present study. Firstly, the chosen spherical deconvolution model faces challenges in accurately estimating the fiber orientation distribution within voxels in the gray matter and cerebrospinal fluid regions. Secondly, it is impossible to entirely avoid the impact of noise. Further work will focus on addressing how to mitigate partial volume effects and reduce the influence of noise on the accuracy of fiber tracking.

V. CONCLUSION

This paper presents a fiber tracking method with adaptive selection of peak direction based on CSD model. The performance of the method was evaluated through quantitative and qualitative comparisons of both Fibercup simulated data and real human brain data. The proposed method demonstrated superior performance in terms of average bundle coverage, smoothness and connections compared to three other CSD model algorithms. Compared to the two algorithms based on the DTI model, our proposed method exhibits a more comprehensive tracking of fiber pathways in regions of fiber crossing and branching, resulting in better tracking outcomes. Therefore, the method proposed in this paper can serve as a

methodological foundation for research, diagnosis, and treatment related to brain disorders resulting from white matter fiber abnormalities or deficiencies.

REFERENCES

[1] S. Mori and P. C. Zijl, "Fiber tracking: principles and strategies - a technical review," *NMR in Biomedicine*, vol. 15, pp. 468-480, 2002.

[2] H. Tamura, N. Kurihara, and Y. Machida, "How does water diffusion in human white matter change following ischemic stroke," *Magnetic Resonance in Medical Sciences*, vol. 8, pp. 121-134, 2009.

[3] M. Maniega, M. Bastin and P. Armitage, "Temporal evolution of water diffusion parameters is different in grey and white matter in human ischaemic stroke," *Journal of Neurology, Neurosurgery and Psychiatry*, vol. 15, pp. 1714-1718, 2004.

[4] J. Zhang, S. Chen and W. Shi, "Effects of xiaoshuan enteric-coated capsule on white and gray matter injury evaluated by diffusion tensor imaging in ischemic stroke," *Cell Transplantation*, vol. 28, pp. 671-683, 2009.

[5] C. K. Tamnes and I. Agartz, "White matter microstructure in early-onset schizophrenia: a systematic review of diffusion tensor imaging studies," *Journal of the American Academy of Child and Adolescent Psychiatry*, vol. 55, pp. 269-279, 2016.

[6] K. E. Schoonover, C. Farmer and A. E. Cash, "Pathology of white matter integrity in three major white matter fasciculi: a post-mortem study of schizophrenia and treatment status," *British Journal of Pharmacology*, vol. 176, pp. 1143-1155, 2019.

[7] Z. O. Toktas, B. Tanrikulu and O. Koban, "Diffusion tensor imaging of cervical spinal cord: a quantitative diagnostic tool in cervical spondylotic myelopathy," *Journal of Craniovertebral Junction and Spine*, vol. 7, pp. 26-30, 2016.

[8] G. Paulina, S. Agnieszka and C. Magdalena, "Retinal nerve fiber and ganglion cell complex layer thicknesses mirror brain atrophy in patients with relapsing-remitting multiple sclerosis," *Restorative Neurology and Neuroscience*, vol. 40, pp. 35-42, 2022.

[9] B. A. Landman, J. A. Bogovic and H. Wan, "Resolution of crossing fibers with constrained compressed sensing using diffusion tensor MRI," *NeuroImage*, vol. 59, pp. 2175-2186, 2012.

[10] A. Ramirez and M. Rivera, "Diffusion basis functions decomposition for estimating white matter intravoxel fiber geometry," *IEEE Transactions on Medical Imaging*, vol. 26, pp. 1091-1102, 2007.

[11] C. Y. Chu, H. P. Huan and C. Y. Sun, "Resolving intravoxel fiber architecture using nonconvex regularized blind compressed sensing," *Physics in Medicine and Biology*, vol. 60, pp. 2339-2354, 2015.

[12] T. E. Behrens, M. W. Woolrich and M. Jenkinson, "Characterization and propagation of uncertainty in diffusion-weighted MR imaging," *Magnetic Resonance in Medicine*, vol. 50, pp. 1077-1088, 2003.

[13] J. D. Tournier, F. Calamante and A. Connelly, "Robust determination of the fiber orientation distribution in diffusion MRI: non-negativity constrained super-resolved spherical deconvolution," *NeuroImage*, vol. 35, pp. 1459-1472, 2007.

[14] J. D. Tournier and F. Calamante, "Direct estimation of the fiber orientation density function from diffusion-weighted MRI data using spherical deconvolution," *NeuroImage*, vol. 23, pp. 1176-1185, 2004.

[15] E. Kaden, T. R. Knosche and A. Anwander, "Parametric spherical deconvolution: inferring anatomical connectivity using diffusion MR imaging," *NeuroImage*, vol. 37, pp. 474-488, 2007.

[16] K. G. Schilling, V. Nath and J. A. Blaber, "Empirical consideration of the effects of acquisition parameters and analysis model on clinically feasible q-ball imaging," *Magnetic Resonance Imaging*, vol. 40, pp. 62-74, 2017.

[17] M. Descoteaux, E. Angelino and S. Fitzgibbons, "Regularized, fast, and robust analytical Q-ball imaging," *Magnetic Resonance in Medicine*, vol. 58, pp. 497-510, 2007.

[18] A. Barmpoutis, M. S. Hwang and D. Howland, "Regularized positive-definite fourth order tensor field estimation from DW-MRI," *NeuroImage*, vol. 45, pp. 153-162, 2009.

[19] T. D. Haije, E. Ozarslan and A. Feragen, "Enforcing necessary non-negativityy constraints for commen diffusion MRI models using sum of squares programming," *NeuroImage*, vol. 209, pp. 116405, 2020.

[20] J. Cheng, R. Deriche and T. Jiang, "Non-negative spherical deconvolution (NNSD) for estimation of fiber orientation distribution function in single-multi-shell diffusion MRI," *NeuroImage*, vol. 101, pp. 750-764, 2014.

[21] R. Marco and S. Henrik, "Fiber continuity based spherical deconvolution in spherical harmonic domain," *Medical Image Computing and Computer-Assisted Intervention*, vol. 16, pp. 493-500, 2013.

[22] M. R. Nazem-Zadeh, E. Davoodi-Bojd and H. Soltanian-Zadeh, "Atlas-based fiber bundle segmentation using principal diffusion directions and spherical harmonic coefficients," *NeuroImage*, vol. 54, pp. 146-164, 2010.

[23] V. Patel, Y. Shi and P. M. Thompson, "Mesh-based spherical deconvolution: a flexible approach to reconstruction of non-negative fiber orientation distributions," *NeuroImage*, vol. 51, pp. 1071-1081, 2010.

[24] F. Calamante and J. D. Tournier, "Track-density imaging (TDI): super-resolution white matter imaging using whole-brain track-density mapping," *NeuroImage*, vol. 53, pp. 1233-1243, 2010.

[25] B. Jeurissen, J. D. Tournier and T. Dhollander, "Multi-tissue constrained spherical deconvolution for improved analysis of multi-shell diffusion MRI data," *NeuroImage*, vol. 103, pp. 411-426, 2014.

[26] J. D. Tournier, F. Calamante and A. Connelly, "MRtrix: diffusion tractography in crossing fiber regions," *International Journal of Imaging Systems and Technology*, vol. 22, pp. 53-66, 2012.

[27] D. M. Morris, K. V. Embleton and G. J. Parker, "Probabilistic fiber tracking: differentiation of connections from chance events," *NeuroImage*, vol. 42, pp. 1329-1339, 2008.

[28] R. E. Smith, J. D. Tournier and F. Calamante, "Anatomically-constrained tractography: Improved diffusion MRI streamlines tractography through effective use of anatomical information," *NeuroImage*, vol. 62, pp. 1924-1938, 2012.

[29] F. Dellacqua, P. Scifo and G. Rizzo, "A modified damped richardson-lucy algorithm to reduce isotropic background effects in spherical deconvolution," *NeuroImage*, vol. 49, pp. 1446-1458, 2010.

[30] F. Dellacqua and P. Scifo, "A model-based deconvolution approach to solve fiber crossing in diffusion-weighted MR imaging," *IEEE Transactions on Biomedical Engineering*, vol. 54, pp. 462-472, 2007.

[31] B. Jeurissen, A. Leemans and D. K. Jones, "Probabilistic fiber tracking using the residual bootstrap with constrained spherical deconvolution," *Human Brain Mapping*, vol. 32, pp. 461-479, 2011.

[32] B. Jeurissen, A. Leemans and J. D. Tournier, "Estimating the number of fiber orientations in diffusion MRI voxels: a constrained spherical deconvolution study," ISMRM, pp. 573, 2010.

[33] S. Mori, B. J. Crain and V. P. Chacko, "Three-dimensional tracking of axonal projections in the brain by magnetic resonance imaging," *Annals of Neurology*, vol. 45, pp. 265-269, 1999.

[34] M. Lazar, D. M. Weinstein and J. S. Tsuruda, "White matter tractography using diffusion tensor deflection," *Human Brain Mapping*, vol. 18, pp. 306-321, 2003.

[35] M. A. Coté, G. Girard and A. Boré, "Tractometer: Towards validation of tractography pipelines," *Medical Image Analysis*, vol. 17, pp. 844-857, 2013.

[36] L. Y. Cai, Q. Yang and P. Kanakaraj, "MASiVar: Multisite, multiscanner, and multisubject acquisitions for studying variability in diffusion weighted MRI," *Magnetic Resonance in Medicine*, vol. 86, pp. 3304-3320, 2021.